Solar Energy Materials and Solar Cells 191 (2019) 316–328

Contents lists available at ScienceDirect

Solar Energy Materials and Solar Cells

journal homepage: www.elsevier.com/locate/solmat

Integration of phenylammoniumiodide (PAI) as a surface coating molecule towards ambient stable $MAPbI_3$ perovskite for solar cell application

K.O. Ogunniran[a,b,*], G. Murugadoss[b,**], R. Thangamuthu[b], J. Karthikeyan[c], P. Murugan[c]

[a] Department of Chemistry, College of Science and Technology, Covenant University, PMB, 1023 Ota, Ogun State, Nigeria
[b] Electrochemical Materials Science Division, CSIR-Central Electrochemical Research Institute, Karaikudi 630003, Tamil Nadu, India
[c] Functional Materials Division, CSIR-Central Electrochemical Research Institute, Karaikudi 630003, Tamil Nadu, India

ARTICLE INFO

Keywords:
Perovskite
PAI
Stability
CuSCN
C-G counter electrode

ABSTRACT

In the present work, different hybrid perovskites were synthesized by gradual concentration variation of larger cation of phenylammoniumiodide (PAI) and methylammoniumiodide (MAI) in PbI_2 solution with the aim of improving the stability of $MAPbI_3$ film and photovoltaic efficiency. To understand the properties of perovskite like structural, optical, thermal, morphological and chemical state, extensive characterizations such as XRD, UV–visible spectroscopy, FE-SEM, SEM, EDX and XPS were performed. The role of PAI was investigated further with the use of DFT studies. The DFT results confirmed that the PAI was passivated on the surface of $MAPbI_3$ with most stable arrangement. The stable arrangement revealed the formation of л-л interactions within the phenyl rings, which shielded the MAI crystals and thereby resulted in enhanced stability of the perovskites. Highly protected perovskite consequently yielded high- performance solar cell device with enhanced stability under 60% humidity, high temperature exposure and longer time stability even when directly exposed to normal room temperature. The new investigation of capping techniques with the use of bigger organic molecules, high performance solar cell with low device costs could emerge. This could lead to unprecedented rapid progress on power conversion efficiency (PCE). Thus, more stable organic-inorganic hybrid perovskites could be developed for future applications.

1. Introduction

The useful application of organic-inorganic perovskites-type pigment around the development of new photovoltaic cells for commercial use has brought new dimensions to material research scientists over the years [1,2]. Various studies have led to discovery of different formation mechanism of organic-inorganic perovskites with remarkable power conversion efficiencies (PCEs) which has displayed increase from 3.8% for methyl ammonium lead halide, $CH_3NH_3PbX_3$ (X = Br, I) in 2009 to more than 20% for $FAPbI_3$-based PSCs in 2015 [3–8]. The organic-inorganic perovskites have been selectively reported to be distinct materials with unique properties such as appropriate band gap, high absorption coefficient, long charge diffusion length and solution processability [9–11]. Based on several positive results [12–15] on their power conversion efficiencies, many efforts have been focused on the commercialization of these new materials to solve global energy challenge. However, it is disappointed to say that most of the perovskites prepared so far have failed to meet the commercial requirements such as stability with high efficiency, low cost and long lifetime durability [16–18].

The physical characteristics of the perovskites depend greatly on the constituents of the ABX_3 [19–22]. The lattice arrangements, which can be represented in multiple ways crystallography, simply allow large atomic or molecular cation (positively-charged) of type A in the centre of the cube. The corners of the cube are occupied by atoms B (also positively-charged cations) while the faces of the cube are occupied by a smaller atom X with negative charge halogen (anion). The electronic band structures of the perovskites are controlled by the electronic orbital of the B and X^- ions [23,24] while the centre A^+ ions determine the symmetry of the perovskite [25]. In addition, the A^+ organic cation stabilized by intercalation of large-sized organic cation, such as n-butylammine or ethane-1,2-diammonium (BA^+ or EDA^{2+}), can further enhance the stability of all-inorganic perovskite [26]. To realize commercial applications of PSCs, the long-term stability issues such as durability under humid, thermal, and light-soaking conditions should be further investigated and improved [27,28]. For the aforementioned

* Corresponding author at: Department of Chemistry, College of Science and Technology, Covenant University, PMB, 1023 Ota, Ogun State, Nigeria.
** Corresponding author.
E-mail addresses: kehinde.ogunniran@covenantuniversity.edu.ng (K.O. Ogunniran), murugadoss_g@yahoo.com (G. Murugadoss).

https://doi.org/10.1016/j.solmat.2018.11.041
Received 15 July 2018; Received in revised form 20 October 2018; Accepted 28 November 2018

reasons, surface passivation strategies of PSCs have been vigorously pursued. For example, Snaith et al. employed various organic Lewis bases such as thiophene and pyridine to passivate the surface of perovskite films to achieve high photovoltaic power conversion efficiency [29] and Lee et al. were fabricated stable perovskite solar cells by incorporation of large 2D phenylethylammonium lead iodide on the grain boundary of the formamidinium lead iodide ($FAPbI_3$) perovskite [30]. But to date, only limited research reported for long-term stability under ambient and light irradiation condition [28–30].

Using various synthetic approach, $MAPbI_3$ have been thoroughly investigated and recently given rise to a PCE approaching 20% [15,31]. However, $MAPbI_3$ is confronted with the problem of low photo and thermal-stability to be commercialized [32,33]. Low crystallization energy and low temperature phase transformation between the tetragonal and cubic phase at ≈ 320 K has been identified as the factors responsible for its unstable nature [34,35]. Therefore, present work aims at using cheaper organic materials to increase the stability of $MAPbI_3$ perovskite by gradual addition of PAI, which is a bigger molecule to fortify the structure with the formation of capped organic cations perovskite. This work was designed to study different ratio of MAI:PAI in order to arrive at the most stable perovskite under ambient temperature. Based on the idea of preparing stable perovskite for commercial solar cell, the present investigation followed simple solution synthetic method to prepare $MAPbI_3$ by addition of different ratio of PAI with the aim of establishing ambient temperature stable organic-inorganic perovskites for future solar cells.

2. Materials and methods

2.1. Reagents

Lead Iodide (PbI_2, 99%), hydroiodic acid (HI, 57% in water), aniline ($C_6H_5NH_2$, 99%) and methylamine (CH_3NH_2, 40% in methanol) and copper (I) thiocyanate (99%), and Titanium diisopropoxide bis(acetylacetonate) solution are purchased from Sigma-Aldrich and used as received without further purification. Propylsulfide purchased from TCI chemical Pvt. Ltd. (98%). Methylammoniumiodide (MAI) (CH_3NH_3I) and phenylammoniumiodide (PAI) ($C_6H_5NH_3I$) were synthesized according to the method previously reported [36–39] (Details information provided in Supplementary data).

2.2. Preparation of perovskite precursors

Solution method was used to prepare the perovskite precursors. 1 M of 461 mg PbI_2 was dissolved in 1 mL of dimethylformamide (DMF) and dimethyl sulfoxide (DMSO) mixed (4:1) solution. However, various concentrations of both MAI and PAI were added together in 1 mL of dimethylformamide (DMF) to make 1 M solution in ratio of N = 1:0, N = 0.9:0.1, N = 0.7:0.3, N = 0.5:0.5, N = 0.3:0.7, N = 0.1:0.9 and N = 0:1 respectively. The solution was stirred for 30 min at 60 °C at ambient atmosphere. For characterization purpose, the precursor obtained was applied to a washed glass substrate on the hot plate (Fig. 1) at 100 °C for 15 min to form thin film perovskite. For device fabrication, the solution was spin coated on the FTO/c-TiO_2/m-TiO_2.

2.3. Perovskite solar cell fabrication

FTO glass (15 Ω/sq) was thoroughly cleaned with detergent, water, acetone and isopropanol in sonicator for 15 min respectively after which it was treated with UV ozone cleaner for 15 min before use. A 50 nm thick dense blocking layer of TiO_2 (bl-TiO_2) was deposited onto the cleaned F-doped SnO_2 substrate by spin coating using a 0.39 mM titanium di-isopropoxide bis (acetylacetonate) solution and then sintered at 120 °C to prevent direct contact between FTO and the hole-conducting layer. Then, a thick mesoporous TiO_2 layer was deposited by spin coating TiO_2 paste (Dyesol 18NR-T) diluted further in ethanol at 1:3.5 with 3000 rpm for 60 s followed by sintered in air at 450 °C for 1 h. The solutions were cool to room temperature, after which they were infiltrated into the mesoporous layer by spin-coating at 2500 rpm for 10 s and at 4000 rpm for 30 s. The substrate was then dried on a hot plate at 100 °C for 15 min before CuSCN HTM layer was deposited on it using doctor blading at 80 °C. The HTM solution was prepared by dissolving 7 mg CuSCN (Kishida Chemical Co. Ltd.) in 1 mL of propylsulfide. Carbon:graphite (1:3) mixture was deposited on another FTO (counter electrode) plate as well as on the FTO/c-TiO_2/m-TiO_2/perovskite/CuSCN film for sandwich type architecture.

2.4. Characterization

The structures of the synthesized methylammonium iodide (MAI) and phenylammonium iodide (PAI) were confirmed with the use of solid state 500 MHz AVANCE III HD Bruker nmr spectrometer. The surface morphology, chemical composition, and structure of the prepared perovskites were characterized using scanning electron microscope (SEM), energy-dispersive X-ray analysis (EDX) (SEM - JEOL JSM-6380LV), JEM 2100F), performed with an acceleration voltage of 200 kV by placing the powder on a copper grid. X-ray diffraction (XRD, Bruker Germany D8 Advance) with Cu Kα radiation (λ = 1.54 Å), was used to collect the data for XRD pattern of the thin film of the perovskite. X-ray photoelectron spectroscopy (XPS) measurements were done on the ESCA + Omicron UK XPS system with a Mg Kα source and a photon energy of 1486.6 eV. The binding energies were referenced to the C 1s peak at 284.6 eV of the surface adventitious carbon. Fourier transformed infrared (FTIR) spectroscopy was performed on a Thermo Nicolet 200 FTIR spectrometer using the KBr wafer technique. A spectrum was collected in the mid-IR range from 400 to 4000 cm^{-1} with a resolution of 1 cm^{-1}. UV–visible absorbance was measured by using Varian Cary 5000 scan UV–VIS NIR double beam spectrophotometer. The thermal decomposition measurements of the prepared sample were determined from the simultaneous thermal analysis (TG/DTA, SDT Q 600 V20) from RT to 1000 °C under nitrogen atmosphere.

We modelled the bulk $CH_3NH_3PbI_3$ structure which is globally (both lattice constant and ions) relaxed using density functional theory (DFT) calculations. The self-consistent procedure was adopted as implemented in Vienna ab initio simulation package (VASP) [40]. In our calculations, the electronic wave functions were expanded using plane waves within projector augmented wave (PAW) pseudo-potential formalism [41]. The electron-electron correlations were corrected by generalized gradient approximations (GGA) [42]. The wave function optimizations were performed with convergence factor of 10^{-6} eV and the ionic relaxations were carried out iteratively until the forces between all the ions became less than 0.01 eV/Å. The (1 1 1) surface slab of $CH_3NH_3PbI_3$ crystals were constructed with periodicity along x and y direction and 15 Å vacuum was kept in z direction to avoid the interaction between the nanostructures and its periodic images. The cell constants of this surface slabs are not optimized but the ions were relaxed with above criteria. For structural relaxation of bulk, it Brillouin zone was sampled with 17 × 17 × 17 Monkhorst Pack k-points while that of (1 1 1) surface slab was gridded with 5 × 5 × 1 Γ centred k-points. The band structures were deduced from non-self-consistent calculations which use the charge density and wave function obtained from the self-consistent calculations.

Photocurrent - voltage (J-V) measurement of PSCs were performed under AM 1.5 sun irradiation (100 mW/cm^2) using a 100–220 W small beam simulator (Photo Emission Tech., Inc., model SS80AAA) with an AM1.5 G filter solar simulator (100 mW/cm^2), and the light intensity was calibrated with a standard Si photodiode detector (Bunkou Keiki, Japan). Incident photon-to-current conversion efficiency (IPCE) measurements were determined using a 300-W xenon light source and a monochromator. The applied voltage scan step = 10 mV and delay time = 200 ms which was followed for all the experiments.

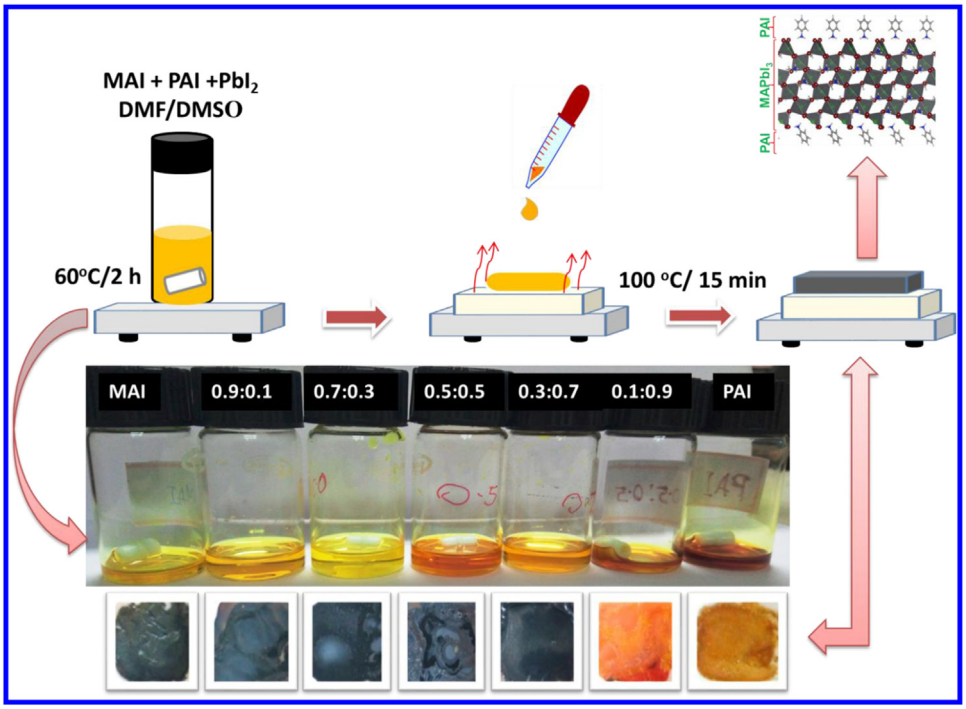

Fig. 1. Schematic illustration of the perovskite solution prepared from different ratio of MAI and PAI by one step method. The photo images show color variation of the perovskite precursor solution and corresponding films with respect to stoichiometric ratio of the MAI and PAI.

3. Results and discussion

This work was carried out by using common chemicals (Hydroiodic acid, methylamine and aniline) and inexpensive techniques to meet the demand for large scale production with low cost. The studies were focused on two directions; (i) study of perovskite on glass substrate to elucidate the structure and morphology of the free perovskites and (ii) depositing the selected perovskite solutions on FTO by spin coating for solar cell fabrication. The structures of methylammonium iodide (CH_3NH_3I, MAI) and phenylammonium iodide ($C_6H_5NH_3I$, PAI) were confirmed with the use of ^1H and ^{13}C NMR studies (Fig. S1a-d). A Simple single step solution processing method was successfully used to prepare perovskites thin film as described in experimental section (Fig. 1). Adoption of one step synthesis through solution method would ensure evenly passivation of bulk molecules of PAI on the surface of $MAPbI_3$ film and yielded new framework pattern. We believe that the existence of new bonding forces played significant role of adducting PAI molecule within bonding in $MAPbI_3$ surface with maximum stability energy as obtained from DFT study. The passivation of larger cation of PA resulted improved stability and device performance [25,37,43,44].

3.1. XRD studies

The perovskite phases were identified with the study of the XRD patterns obtained after annealing on the hot plate for 15 min. The XRD patterns obtained for different concentrations of PAI mixed with $MAPbI_3$ perovskites are shown in Fig. 2a. The diffraction spectrum for $CH_3NH_3PbI_3$ is in good agreement with the literature values with indexed peaks of 110 (13°.99′), 112 (19°.93′), 202 (24°.44′), 220 (28°.26′) and 222 (31°.68′), thus confirmed the formation of perovskite phase with cubic structure [36,45,46]. The sharp and high intensities of the signals confirmed good crystallinity of the perovskite films. The peaks appeared in the XRD spectra corresponds to 0.9:0.1, 0.7:0.3, 0.5:0.5 and 0.3:0.7 compositions. The perovskite phase (1 1 0) was observed at 14°.43′, few additional diffraction peaks were observed only at higher concentration (0.1:0.9 of the MAI to PAI) and tend towards pure $PAPbI_3$ perovskites. The absence of $PAPbI_3$ related diffraction peak in the lower concentrations is reflecting that no substitution of PA cation with replacement of MA in the cubic structure. It may due to huge variation of the ionic radius of MA (~3.0 Å) and PA (5.89 Å). The peak position was not changed with respect to the concentration, the result also shows that the PA was not substituted in the cubic structure of $MAPbI_3$. The absence of lead iodide peak in the XRD pattern for 0.5:0.5 concentration reflects high purity with good stability at ambient atmosphere. Lower concentration is also possible but may lead to a distorted cubic structure [19,37].

3.2. Optical properties study

The UV–visible absorption spectra of the perovskite films are presented in Fig. 2b. As observed in the spectra, strong electronic absorption peaks were obtained for the perovskite thin films at about 780 nm and ≈ 500 nm. The peak at ≈ 770 nm was attributed to band-edge electronic transition [45,47]. To predict the suitability of the perovskites for solar cell application, the band gap energies of the films were estimated from the optical reflectance data by the Kubelka–Munk's method with the use of graph plotted between [K/S] and hv. The intercepts obtained were considered as the band gap energies of the perovskites (Fig. S2a, b). The band gap energies of $MAPbI_3$ and $PAPbI_3$ perovskites were found to be 1.51 and 2.32 eV, respectively. The band gap energies of 0.9:0.1, 0.7:0.3 and 0.5:0.5 compositions were found to be between 1.51 and 1.55 eV. No obvious changes observed in band gap with respect to the concentrations of PAI. Slightly increased band gap value (higher than $MAPbI_3$) obtained for the higher concentration (0.9:0.1). It may be due to formation of little PAI phase along with MAI which is in agreements with XRD result.

3.3. Fourier transform infrared spectroscopy (FT-IR) studies

Fourier transform infrared spectroscopy (FTIR) provided clarification to the composition of the perovskite thin films (Fig. S2c). The spectra assignments are presented in Table 1. In the spectrum of $MAPbI_3$, strong absorption bands observed at 2824 and 1454 cm^{-1} were attributed to CH *str.* and *bending* of CH_3 in $CH_3NH_3PbI_3$,

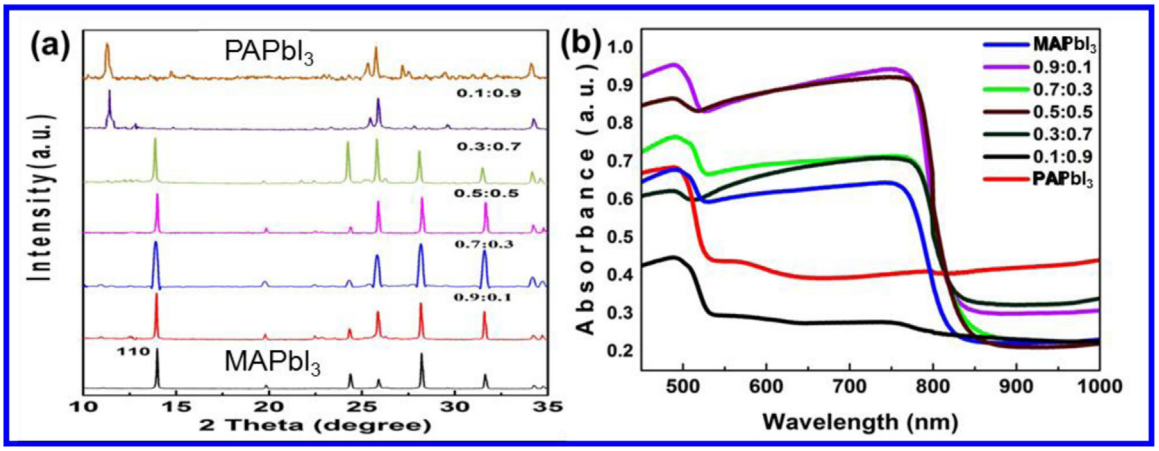

Fig. 2. (a) XRD patterns between 10° and 35° show characteristic peaks of $MAPbI_3$ and $PAPbI_3$. (b) Optical absorption spectra of the perovskite thin films at ambient temperature.

Table 1
Device performance of the $MAPbI_3$, 0.5:0.5 and $PAPbI_3$ perovskites.

Perovskites	J_{sc}/(mA cm^{-2})	V_{oc}/V	Fill Factor (FF)	Efficiency (Ƞ)/%
$PAPbI_3$	5.94	0.69	58.40	2.39
$MAPbI_3$	20.60	0.89	55.64	10.25
0.5:0.5	24.42	0.93	49.75	11.38

respectively while the medium band at 3233 cm^{-1} was assigned to NH *str*. of NH_3 [46,48–51]. However, the presence of both CH *str*. aliphatic and aromatic were found in the spectra of the perovskites with varying ratio of MAI/PAI within the range of 2995–3006 cm^{-1} and ≈ 3130 cm^{-1}, respectively. Also, the bands at ≈ 1450 cm^{-1} in the spectra were assigned to CH_3 *bending*. The C = C ar. *str* was found within ≈ 1590–1669 cm^{-1}. As expected, only CH *str*. aromatic appeared in the spectrum of $PAPbI_3$ at 3187 cm^{-1} with C = C *str*. aromatic at ≈ 1454–1590 cm^{-1}. The FT-IR spectroscopy supported the presence of MA and PA in the perovskites films with increase in intensity as the ratio increases.

3.4. Morphology studies

In order to understand the structural arrangement of perovskite thin films, 1 cm^2 sectional area of pure $MAPbI_3$, 0.5:0.5 and pure $PAPbI_3$ were studied with field emission scanning electron microscopy (FE-SEM). The thin films were prepared by drop casting method. From the images obtained at different magnifications, $MAPbI_3$ (Fig. S3a-c) shows relatively rod-like asymmetric structure spreading out from a central point on the plate while $PAPbI_3$ (Fig. S3g-i) displays particles with wide surface arranged in layers with interlocking network structure in-between. However, the two morphologies were observed in 0.5:0.5 thin film forming interlocking phase that identified with the morphologies of the perovskite. The new morphology shows area covered with rod shapes while another area displays coiled layers network. This confirmed the presence of both moieties in 0.5:0.5 mixed perovskite phase. To further affirm the presence of both $MAPbI_3$ and $PAPbI_3$ in 0.5:0.5 perovskite phase, we further studied the morphology of the black phase of the perovskite in powdery form after scraping it from the surface of the glass substrate using energy dispersion scan electron microscopy. The SEM images from the scraped perovskite (Fig. S4a-c) confirmed $MAPbI_3$ to be rod shaped with average length of 6.69 μm and average diameter of 0.73 μm. We observed non-symmetrical pores within the bulk of the perovskite powder based on the non-alignment of the rods shape. This might be an advantage for $PAPbI_3$ to diffuse into the $MAPbI_3$ spheres. The SEM image for $PAPbI_3$ shows sheet morphology arranged in layers (Fig. S4d-f). However, the SEM image of 0.5:0.5 ($MA_{0.5}PA_{0.5}PbI_3$) confirmed the presence of rod and sheet morphology (Fig. S4h-i).

3.5. Elemental composition

The major constituent elements in the samples were investigated through energy-dispersive X-ray analysis (EDX). Fig. S5a,c,e shows the EDX spectra of the selected perovskites, which established % weight of the constituent elements. It can be concluded that % weights obtained agree with the proposed molecular formulae of the perovskites. For more clarity, the % weights obtained (experimental and calculated) are represented in stacked column bar chart (Fig. S5b,d,f).

Further element status of the perovskites was carried out using X-ray photoelectron spectroscopy (XPS). The results of X-ray photoelectron spectroscopy of $MAPbI_3$, 0.5:0.5 and 0.7:0.3 perovskites are presented in Fig. 3(a-d). The typical survey spectra of $MAPbI_3$, 0.5:0.5 and 0.7:0.3 (Fig. 3a,b) reveal the presence of C (1 s), N (Is), I (3d) and Pb (4f). The binding energies observed for 0.5:0.5 and 0.7:0.3 fell within the same region with insignificant difference of 0.2–0.7 eV for Pb 4f and 0.1–0.3 eV for I 3d compared to pure $MAPbI_3$. The binding energy (BE) for the Pb $4f_{7/2}$ in $MAPbI_3$ was found to be ≈ 137.5 eV while those of 0.5:0.5 and 0.7:0.3 were found to be ≈ 137.1 and 136.6 eV, respectively. The spectra for Pb 4f (Fig. 3c) show well-separated spin-orbit components with separation of about 4.9 eV which is typical of Pb^{2+} ion. Fig. 3(d) shows the I 3d spectra for MAI, 0.5:0.5 and 0.7:0.3 with well-separated spin-orbit components with a separation of about 11.5 eV, which is coherent with characteristic of I^- ion. [52,53]. The spectra indicated that the chemical bonding was not affected in the process of perovskite formation which is in good agreement with XRD pattern obtained.

3.6. Moisture stability study

One of the major causes of instability in the perovskite materials is humidity because perovskite materials such as $CH_3NH_3PbI_3$ are hygroscopic in nature. It readily decomposes into CH_3NH_3I and PbI_2 in the presence of water [54–56]. In our quest to understand the effect of introducing PA moiety on the ambient and phase stability of $MAPbI_3$, selected perovskite films ($MAPbI_3$, 0.9:0.1, 0.7:0.3 and 0.5:0.5) were kept at normal room temperature with about 70% relative humidity for maximum of 30 days. The comparative studies were carried out using visual observation, UV–visible absorption and XRD measurements. Fig. 4(a-d) shows the XRD pattern obtained after aged 5D, 10D and 30D for $MAPbI_3$, 0.9:0.1, 0.7:0.3 and 0.5:0.5 samples, respectively while Fig. 4(e,f) shows the UV–visible spectra obtained after 10D and 30D, respectively. Fig. 4(g) shows the photograph of the thin films on the

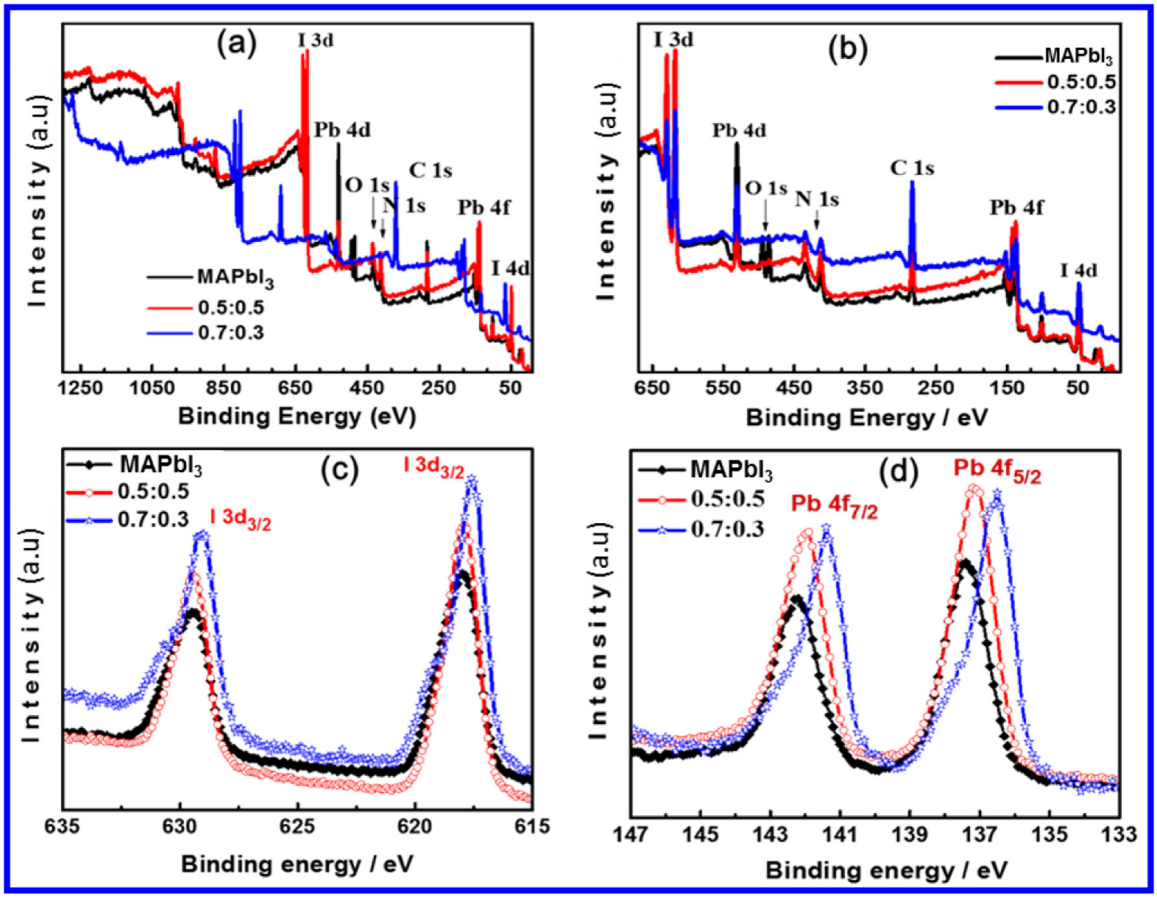

Fig. 3. XPS spectra of pure $MAPbI_3$ and different concentrations of MAI and PAI mixed (0.5:0.5 and 0.7:0.3) thin films: (a) Full survey spectra, (b) expanded full survey spectra, (c) Pb 4f spectra and (d) I 3d XPS spectra.

glass substrate at initial and 30D, respectively for the selected perovskites. It was observed that MAI decomposed black to yellow phase after 30D in ambient temperature. In agreement with the visual observation, XRD pattern obtained shows proportional increase in the characteristic peak for PbI_2 (1 1 0) even though there are still some tiny spots of black phases of the perovskite present as obtained in the XRD pattern. However, XRD pattern for films with varying $PAPbI_3$ shows slight decomposition which is displayed with low intensity of PbI_2 characteristic peak after 30D. This indicates, that the black perovskite phase persisted after 30D of exposure. Thus, the PA molecules serves as protective agent for $MAPbI_3$ cavity and therefore increases its stability as PbI_2 was held firmly within the perovskite thin film. The presence of phenyl group protected the surface of the $MAPbI_3$ by shielding it against reaction with atmospheric oxygen and water molecules; it would be clearly demonstrated later by DFT structural evaluation. Hence, the PA passivated $MAPbI_3$ perovskites possess good stability under high humidity than pure $MAPbI_3$. The UV–visible spectra displayed absorbance with higher intensities as compared to initial UV–-visible spectrum (Fig. 4e,f). The higher intensity of absorption peaks for mixed perovskite revealed well crystalline nature which is in good agreement with XRD results.

3.7. Light stability

Prolonged light illumination in air has been identified as one of the major causes of decomposition of $CH_3NH_3PbI_3$ perovskite [57,58]. Under light illumination, $CH_3NH_3PbI_3$ perovskite decomposes to PbI_2, CH_3NH_2 and HI. Thus, the efficiency reduces gradually as the degradation increases. To understand the effect of PAI on $MAPbI_3$ upon exposure to strong beam of light, selected perovskites ($MAPbI_3$, 0.9:0.1, 0.7:0.3 and 0.5:0.5) were illuminated with 60 W tungsten lamp at 10 cm distance for 72 h. Fig. 5a-d shows the XRD patterns and UV–visible spectra obtained from the thin films after the illumination. The XRD patterns ascertained the stability of PA passivated perovskites (0.9:0.1, 0.7:0.3 and 0.5:0.5) with the persistence perovskite phase peak than in $MAPbI_3$. Higher intensity characteristics peak of PbI_2 was observed in the XRD pattern of $MAPbI_3$. This shows that more PbI_2 decomposed within $MAPbI_3$ perovskite under direct illumination from beam of tungsten light. In contrary, PA passivated perovskites showed little degree of decomposition which decreases as the concentration of PAI in the perovskite increases thus confirming $PAPbI_3$ as light stability enhancement agent. The electronic transitions within the thin films (Fig. 5e) remain higher due to availability of PbI_2 molecules within the electronic sphere to transmit more electrons. It can be concluded that the capping of $MAPbI_3$ with PAI reduced the decomposition of PbI_2.

3.8. Thermal stability

The thermal degradation of organic–inorganic perovskite materials is accelerated under high temperatures. Previous reports showed that $MAPbI_3$ decomposes at a temperature of 230 °C [40,41,55,59]. To further study the impact of PAI with $MAPbI_3$ on stability, thermal gravimetric analysis (TGA) was used to study the thermal stability of perovskites by weight loss [40,42]. Also, XRD patterns and UV–visible spectra were obtained at high temperature for pure $MAPbI_3$, 0.9:0.1, 0.7:0.3 and 0.5:0.5 thin films. Fig. 6(a-d) shows the XRD patterns for $MAPbI_3$, 0.9:0.1, 0.7:0.3 and 0.5:0.5 thin films at 140, 180 and 220 °C respectively along with the photograph of the thin film after direct heating on hot plate. XRD patterns for $MAPbI_3$ thin film (Fig. 6a) reveals gradual degradation of perovskite phase to completely charred

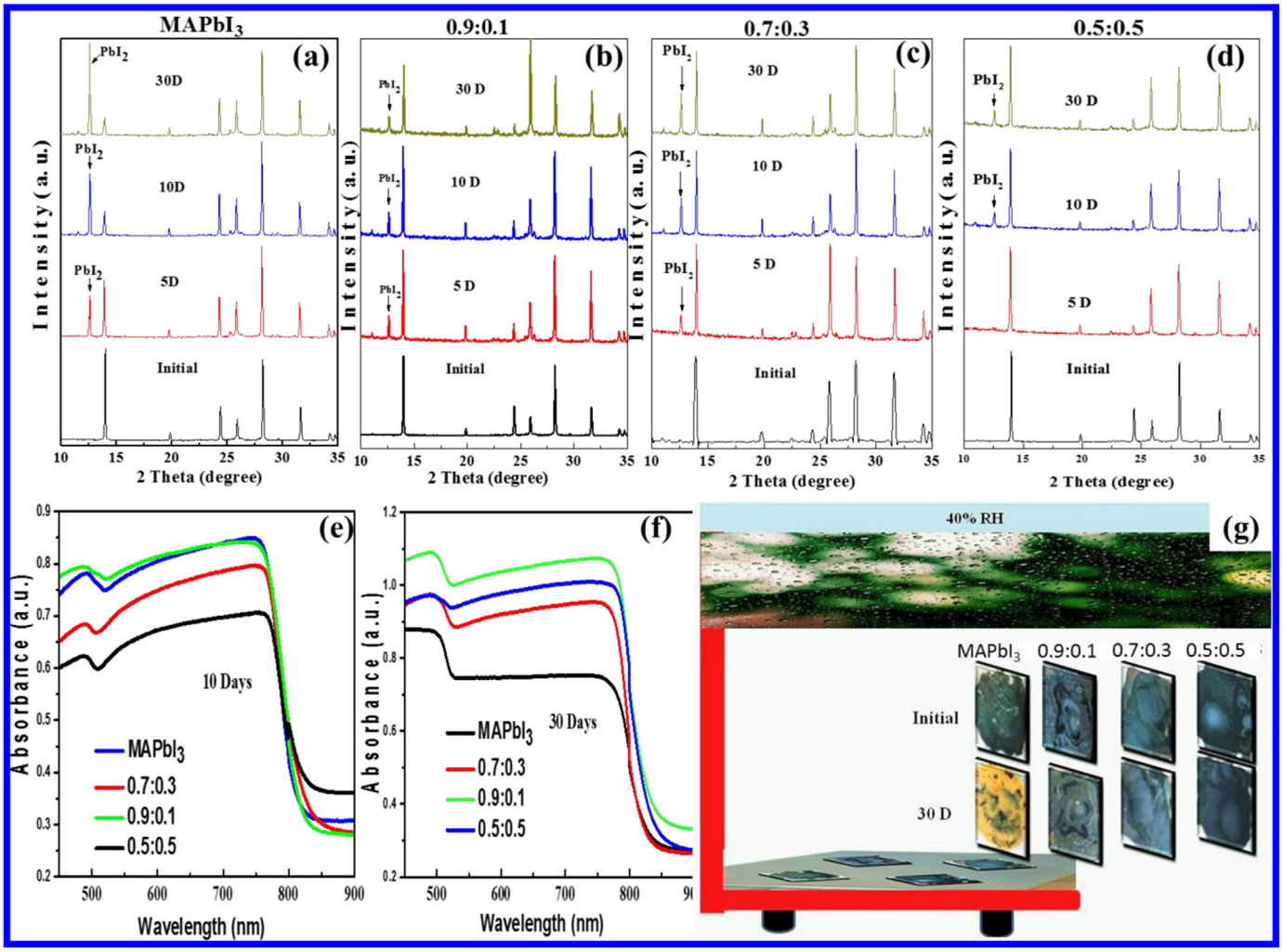

Fig. 4. Stability studies of the effect of relative humidity of 70 ± 5% on the perovskite thin films after storage at ambient temperature for up to 30 days after formation: XRD patterns of the perovskite thin films stored at different days such 5D, 10D and 30D, (a) $MAPbI_3$ and different concentrations of MAI and PAI mixed perovskite (b) 0.9:0.1 (c) 0.7:0.3 (d) 0.5:0.5 films. UV–Visible spectra of the corresponding sample (e) 10D (f) 30D stored at ambient temperature (g) Photographs of the perovskite films as prepared and after 30D of storage in ambient condition.

PbI_2 as the temperature increases from 140 to 220 °C. However, from the XRD patterns of the double organic perovskites (Fig. 6b-d), we observed partial decomposition of PbI_2 from the perovskite phase as the temperature increases but the perovskite phase remains persistence within the temperature range studied. XRD patterns for 0.5:0.5 perovskite thin film (Fig. 6d) shows the perovskite to be the most stable with the appearance of weak PbI_2 related peak as the temperature increases. The conclusion from the XRD patterns is corroborated by the UV–visible spectra obtained for the perovskites. Fig. 7(a,b) shows the electronic transitions spectra for $MAPbI_3$, 0.9:0.1, 0.7:0.3 and 0.5:0.5 perovskite thin films at 180 and 220 °C, respectively. UU-Visible spectrum for $MAPbI_3$ at 180 °C confirmed the presence of the perovskite phase in the thin film with absorption at 780 nm. The thin film decomposed to pure PbI_2 phase at 220 °C with the disappearance of absorption at ≈ 780 nm and appearance of strong PbI_2 characteristic absorption at ≈ 570 nm. However, double organic perovskites (0.9:0.1, 0.7:0.3 and 0.5:0.5) shows strong absorption at ≈ 780 nm with weak PbI_2 characteristic absorption at ≈ 570 nm at 180 and 220 °C, respectively. Thus, the observation confirmed the stability of the $MAPbI_3$ fortified with PA organics. Thermogravimetric analysis reveals the gradual weight loss that occurred within the perovskite moiety as the heating temperature increases. Fig. S4(a-d) reveals the decomposition step of $MAPbI_3$, 0.9:0.1, 0.7:0.3 and 0.5:0.5 as follow:

$$C_6H_5NH_3/CH_3NH_3PbI_3 \rightarrow HI + C_6H_5/CH_3NH_2 + PbI_2$$

The thermographs show that sublimation of HI occurs between 103 and 121 °C for $MAPbI_3$, 0.9:0.1 and 0.9:0.1 while 0.5: 0.5 composition remains stable up to 243 °C. Also, the PbI_2 constituent started to decompose at around 700 °C in 0.5:0.5 while it decomposes below 600 °C in $MAPbI_3$ and other mixed perovskites. The TGA result revealed that about 70% of the organic constituents of the $MAPbI_3$ capped with PA were stable up to 650 °C. The thermograph result shows that the arrangement of pure $PAPbI_3$ and $MAPbI_3$ in 0.5:0.5 is different from the arrangement in the other double organic composition. The result aligned with XRD patterns and UV–visible spectra obtained.

3.9. DFT studies

For better understanding of the role of PA on the improved stability of 0.5:0.5 film, we decided to explore density functional theory (DFT) simulation using Vienna ab initio simulation package (VASP) [60–62]. Based on the results of our characterizations, we concluded that we have obtained more stable 0.5:0.5 film because of presence of PA with $MAPbI_3$, probably by substitution. However, DFT studies reveal the nature of the binding and position of substitution within $MAPbI_3$. We begin by relaxing all the ions in the bulk structure of $MAPbI_3$ perovskite which crystallized in cubic form (Fig. 8a) with the lattice parameters of

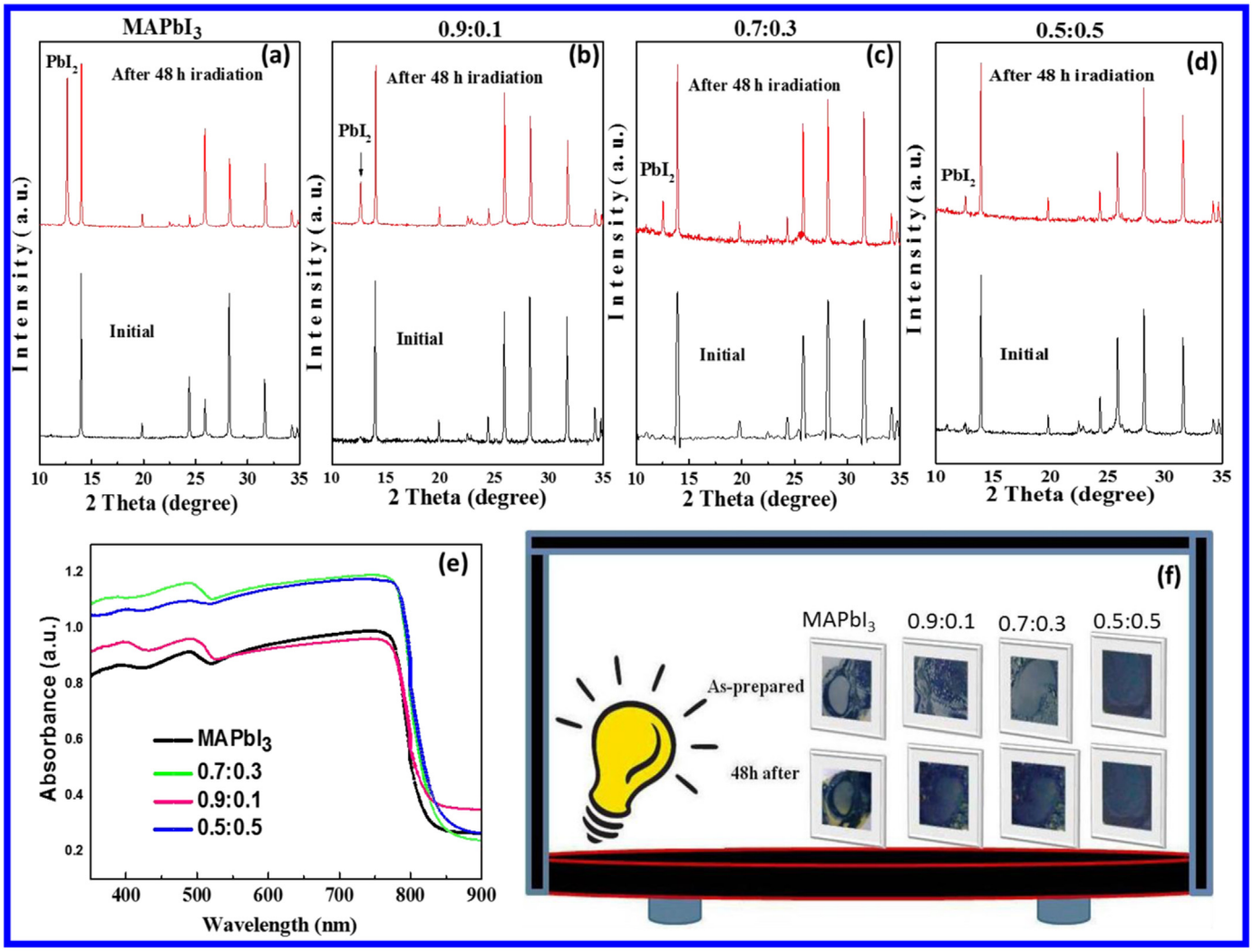

Fig. 5. Stability studies of the perovskite thin films: XRD pattern of (a) $MAPbI_3$, different concentrations of MAI and PAI mixed perovskites, (b) 0.9:0.1, (c) 0.7: 0.3 and (d) 0.5:0.5 as-prepared and after 48 h light irradiation, (e) UV–visible spectra of the corresponding samples after 48 h irradiation, (f) Photograph of the thin films as-prepared and after 48 h light irradiation.

$a = b = c = 6.28$ Å and $\alpha = \beta = \gamma = 90°$. Furthermore, the cell parameters and ions were relaxed to study the ground state structure. It was found that the calculated lattice parameters are $a = 6.43$ Å, $b = 6.37$ Å and $c = 6.51$ Å and $\alpha = \beta = \gamma = 90°$. It clearly indicated the possibility of distortion in cubic structure and the distorted structure is stable by 0.11 eV per formula unit when compared to non-distorted one (Fig. 8b). In this structure, PbI_3 forms corner shared octahedral networks and CH_3NH_3 present in the cuboctahedra site. The Pb-I bond distance varies from 3.10 to 3.35 Å and C-H, N-H, and C-N bond distances are 1.10, 1.03 Å, and 1.46 Å, respectively. The meta-stability of this crystal in the presence of moisture leads to poor durability of the solar cell. To overcome this issue, we have used organic molecules as a capping molecule to protect the surface of the $MAPbI_3$ from the moisture. In this work, we have used phenyl ammonium $C_6H_5NH_3$ (PA) as anchoring molecule to protect the surface. However, we doubted the possibility of formation of perovskite structure with this molecule. Hence, we replaced the methyl ammonium (MA) by PA molecule in the same perovskite structure and similar calculations were carried out with complete relaxation of both lattice parameters and ions. From the study, we confirmed that phenyl ammonium lead tri-iodide will not substitute inside $MAPbI_3$ lattice because the optimized structure shows few broken Pb-I bonds in highly distorted Pb-I network, owing to the larger size of the PA molecule (5.89 Å) as compare to that of MA (~3.00 Å). The minimum and maximum I - I distances in PbI_3 network are 6.40 Å and 9.22 Å, respectively and after subtracting diameters of I^-, it was found to be highly difference (3.86 Å) from the maximum I - I distance. Since organic molecule can get maximum of 5.36 Å along the diagonal distance between the opposite edges, PA molecules cannot enter $MAPbI_3$ perovskite structure.

Since the distortion energy is small, we have used the cubic $MAPbI_3$ to model (1 1 1) surface slabs. This surface is one of the stable surfaces with closed pack atomic structure. The surface slab can mimic the properties of the surface of perovskite particles. In the stoichiometric slab, it was found that Pb atoms will be in excess on one side while iodine atoms will be in excess on the other side. In Pb excess side, the Pb atoms have three coordination sites through which bond is formed with I atoms below. Instead, in the non-stoichiometric surface with two PA molecules, we removed one MA molecule on the surface and an iodine atom was added to compensate the charges for the whole system. The iodine atoms can be moved from the I rich side to Pb rich side to retain five coordination for all the Pb atoms. This model was found to be structurally stable (Fig. 8b, c). Also, from the XPS studies, it is found that the I atoms are excess in the system, thus our model is valid.

To further check the feasible adsorption configuration of PA over (1 1 1) surface of $MAPbI_3$, we have anchored two PA molecules on this surface with different configurations. From this study, we understood that the ammonium group of PA prefers to interact with surface with the interaction energy of 4.76 eV per PA molecule. It clearly shows that

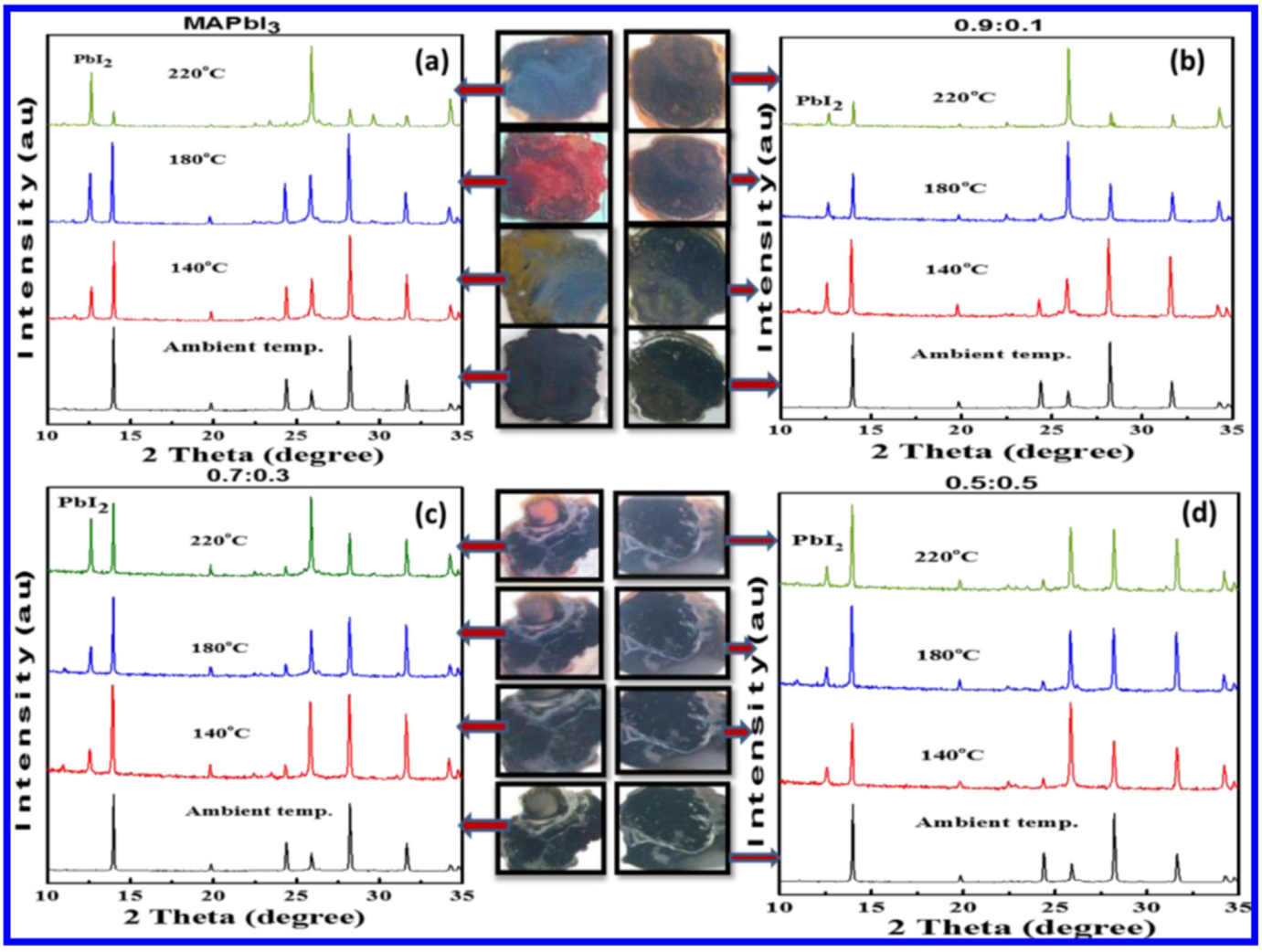

Fig. 6. XRD patterns (a) $MAPbI_3$ (b) 0.9:0.1, (c) 0.7:0.3 and (d) 0.5:0.5 concentrations of MAI and PAI mixed perovskites films at ambient temperature, 140, 180 and 220 °C along with the photographs of the thin films.

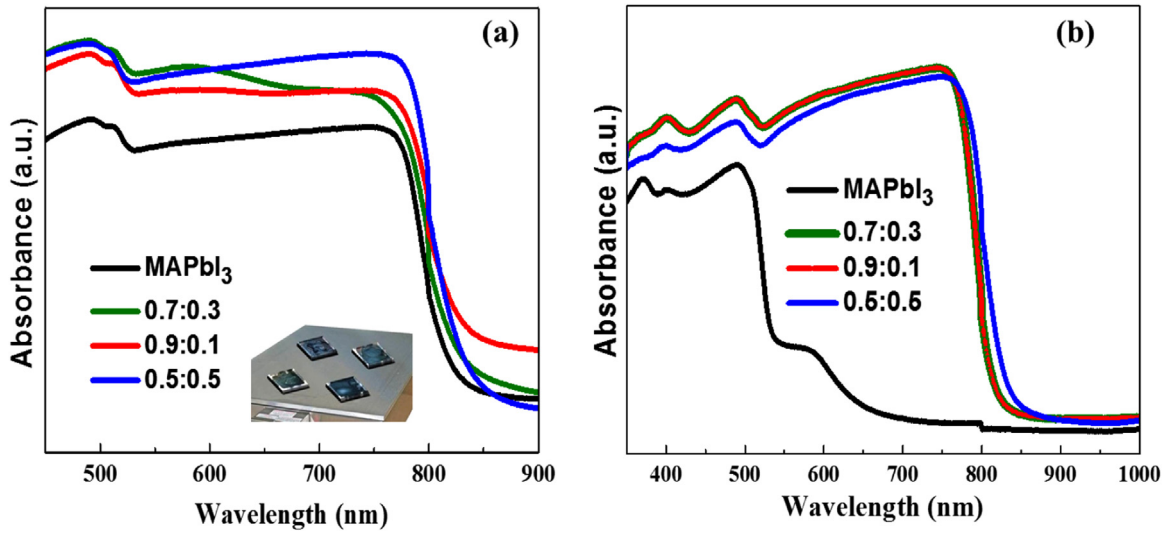

Fig. 7. UV–Visible absorption spectra of $MAPbI_3$, 0.9:0.1, 0.7:0.3 and 0.5:0.5 concentrations of MAI and PAI mixed perovskites thin films (a) temperature at 180 °C and (b) at 220 °C for 30 min.

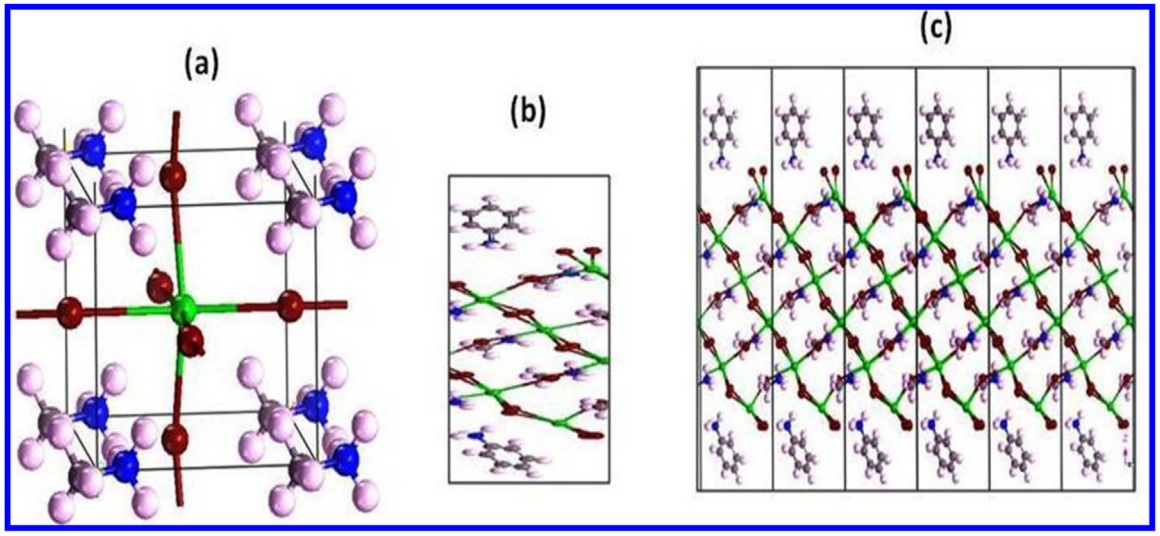

Fig. 8. (a) Ball and stick model of optimized structure of $CH_3NH_3PbI_3$. (b) Optimized structure of PA anchored $CH_3NH_3PbI_3$ representing unit cell. (c) Combine unit cells of optimized structure of PA anchored $CH_3NH_3PbI_3$, black lines represent the boundary of unit cell. Note: green, red, grey, blue and pale white coloured balls represent lead, iodine, carbon, nitrogen, and hydrogen atoms, respectively.

these molecules are strongly interacting with the surface. Thus, it is proven that the (1 1 1) surface of $MAPbI_3$ is strongly protected by molecule by tending outward the benzene group of PA which increase the hydrophobic nature. However, further detail of electronic properties (Fig. S7), valence band and conduction band states (Fig. S8) are provided in the Supplementary information.

3.10. Photovoltaic studies

The top view photograph images of $MAPbI_3$, 0.5:0.5 and $PAPbI_3$ perovskite spin coated on the FTO plates and corresponding scanning electron microscopy images are shown in Fig. 9(a-c). Fig. 9a shows surface view of $MAPbI_3$ perovskite with compact arrangement of cubic particles. The surface view of $PAPbI_3$ (Fig. 9b) shows 0.5:0.5 of the two perovskites with close packed grains. Fig. 9c reveals the formation of porous flower like particles on FTO surface.

The corresponding UV–Vis absorption and X-ray diffraction patterns of perovskites are displayed in Fig. 9(d,e), respectively. UV–Vis absorption shows that 0.5:0.5 perovskite is more optical active than pure $MAPbI_3$ with strong absorption observed at around 780 nm while $PAPbI_3$ shows absorption peak at shorter wavelength region. XRD pattern of the perovskite also revealed perovskite black phase formation for both 0.5:0.5 and $MAPbI_3$ with the (1 1 0) peak at 14.03° while PAI displayed yellow phase of PbI_2 at 12.57 and 11.37° indicating the lack of perovskite phase as proposed in DFT studies.The cross-sectional images with different magnifications of the device (0.5:0.5) are shown in Fig. 9(f) and (g).

To understand photovoltaic efficiency, the selected three perovskites were applied for device fabrication. Cost effective carbon with graphite (C:G) mixture (1:3) was used as contact layer for sandwich type architecture (Fig. 10). In addition, highly stable solid-state based copper (I) thiocyanate (CuSCN) thin film applied as hole transport materials [26,36,63,64]. The solar cells were fabricated for $MAPbI_3$, 0.5:0.5 and $PAPbI_3$ using sandwich method as FTO/TiO_2/$(PA)_{0.5}(MA)_{0.5}PbI_3$/CuSCN/C:G/FTO device structure to study photovoltaic properties. The device structure and photovoltaic characteristics of the devices are shown in Fig. 10(a-e). The detailed photovoltaic parameters obtained are as summarized in Table 1. The results show that 0.5:0.5 device displays the best PCE of 11.38, a V_{oc} of 0.93 V, current density of 24.42 mA cm^{-2} and fill factor of 49.75% as compared to $MAPbI_3$ device with PCE of 10.25, a V_{oc} of 0.89 V, current density of 20.60 mA cm^{-2} and fill factor of 55.64%. $PAPbI_3$ device displays the lowest efficiency of 2.39%, V_{oc} of 0.69 V, current density of 5.94 mA cm^{-2} and fill factor of 58.40%. The photocurrent density-voltage results clearly demonstrated that the role of PA on the $MAPbI_3$ providing surface protection to the cubic structure of the $MAPbI_3$ in the perovskite which resulted in enhanced photovoltaic properties of $MAPbI_3$ perovskite. The presence of phenyl rings on the surface layer was proposed to set π-π bonds which could be hydrophobic in nature to serve as shielding layer around the cubic structure of $MAPbI_3$. This stabilizes the structure of the perovskite in 0.5:0.5 device to produce better efficiency. Even though our experiment was carried out under 60% relative humidity, yet we were able to obtain 11.38% efficiency for the new protected perovskite (Fig. 10c). This indicates that much higher efficiency would be achieved with the new compound if the device is to be fabricated under very low humidity condition with other organic HTM and Au as contact layer. Thus, we can say that the stability of the new perovskite is responsible for increased efficiency observed in the device. The IPCE spectrum of < FTO/bl-TiO_2/m-TiO_2/$(MA)_{0.5}(PA)_{0.5}PbI_3$/CuSCN/FTO > which specifies the ratio of extracted electrons to incident photons at a given wavelength is shown in Fig. 10(d). The device shows IPCE of about 78% which is higher than that of $MAPbI_3$ devices in literatures [17,64,65]. The value well agrees with the value obtained in the *J–V* curve. The high photon-to-electron conversion of the fabricated device is also demonstrated with the presence of a plateau across 400–780 nm. The protective effect of PA on $MAPbI_3$ is further evidenced with the stability plot shown in Fig. 10(e). The presence of phenyl rings on the surface layer maintained over 90% of initial PCE after been stored in about 60% relative humidity for 250 h without encapsulation. However, the stability of pure $MAPbI_3$ degraded to nearly 40% of its initial PCE after the 250 h. The hysteresis effect at equal concentration of PAI and MAI mixed perovskite investigated as shown in Fig. S9. To quantify the hysteresis effect, a dimensional hysteric index (HI) is introduced [27],

$$HI = \frac{J_{RS}(0.8V_{OC}) - J_{FS}(0.8V_{OC})}{J_{RS}(0.8V_{OC})}$$

where J_{RS} $(0.8V_{oc})$ and J_{FS} $(0.8V_{oc})$ stand for the photocurrent density at 80% of V_{oc} for the RS and FS, respectively. A lower HI corresponds to cells without significant hysteresis, while a higher HI corresponds to hysteretic devices. The calculated hysteresis index value 0.095. The reason for the hysteresis behavior possibly stems from unbalanced charge transportation and collection, the perovskite's ferroelectricity, ion migration, or defects [65].

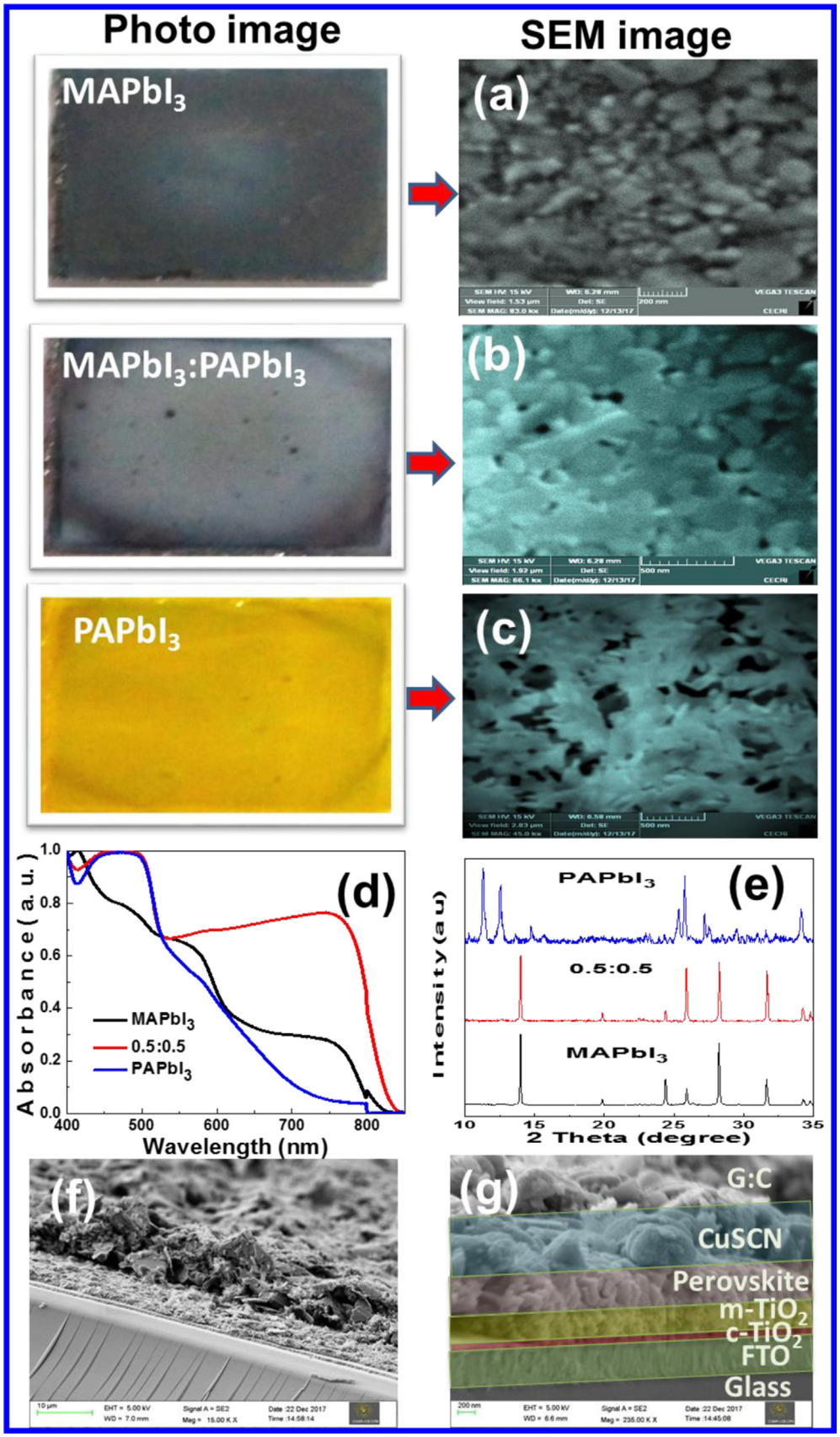

Fig. 9. (a-c) shows the top view SEM images of pure $MAPbI_3$, MAI and PAI mixed (0.5:0.5) and pure $PAPbI_3$ perovskites deposited on FTO/TiO_2 film along with their photographs. The films show uniform and close packed perovskite crystals distribution at higher magnification of mixed (0.5:0.5) perovskite film. (d and e) shows the UV–vis absorption spectra and XRD patterns of perovskites on the FTO/TiO_2 substrates, respectively. Cross-sectional images with different magnifications of the device (0.5:0.5) are displayed in (f) and (g).

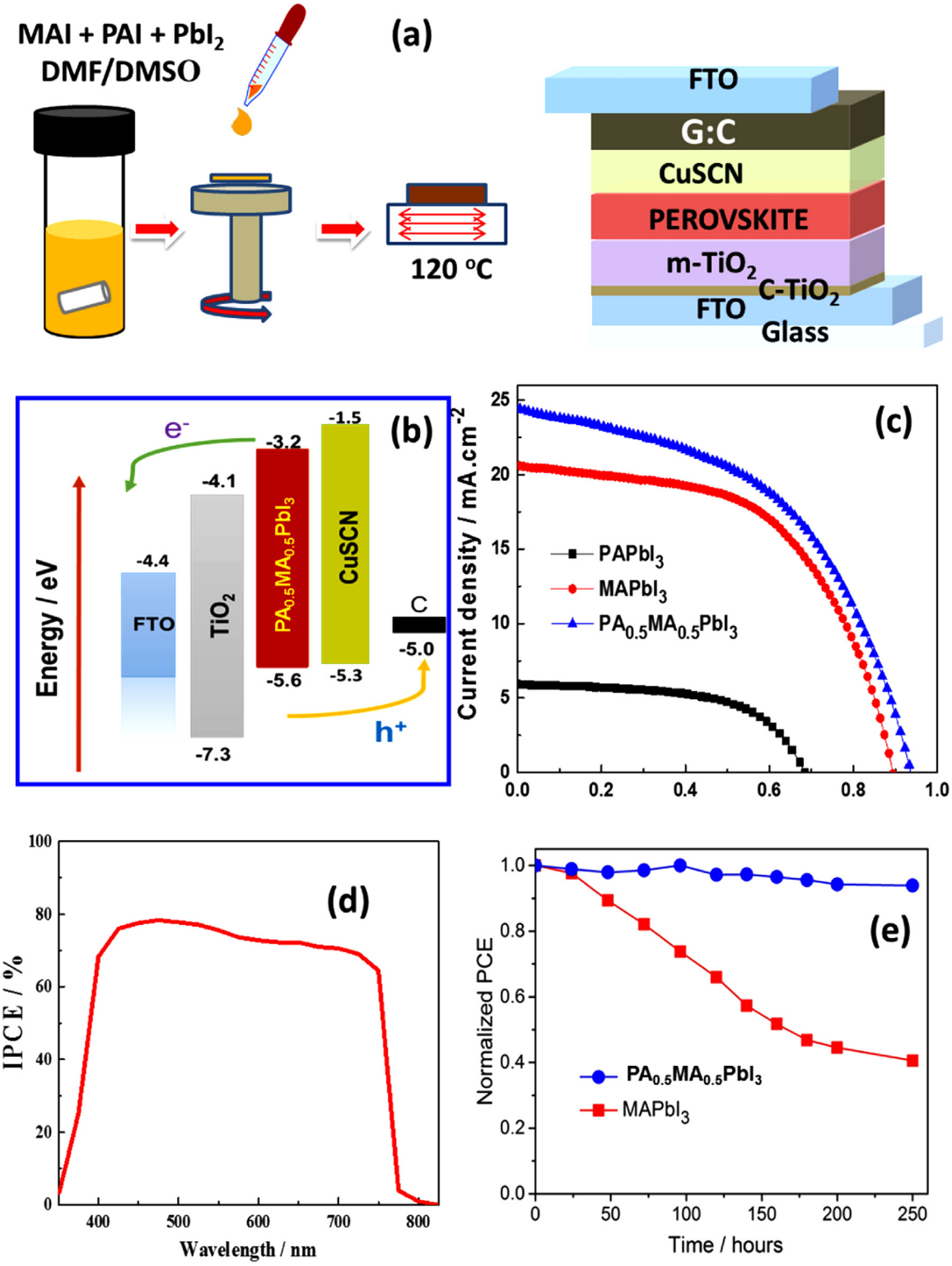

Fig. 10. (a) The schematic diagram for preparation of the devices through spin coating showing coating arrangement for the devices. (b) The energy level diagram of the studied device with a structure of < FTO/bl-TiO_2/m-TiO_2/$(PA)_{0.5}(MA)_{0.5}PbI_3$/CuSCN/FTO > (c) The *J–V* curve, (d) IPCE spectra, and (e) The stability evolution of the derived PSCs performance curve of $(PA)_{0.5}(MA)_{0.5}PbI_3$ and $MAPbI_3$ measured under a constant bias of 0.89 V near the maximum power point.

4. Conclusion

We carefully investigated the moisture, light and thermal stability of the $MAPbI_3$ perovskite by passivation of large ionic radius PA molecule on the surface, which was reported with a better stability than the pure $MAPbI_3$, as well as higher photovoltaic performances. From the extensive characterizations and DFT computational studies, we confirmed that PA molecules did not actually substituted into the $MAPbI_3$. Instead we observed surface interaction leading to capping of $MAPbI_3$ molecules in the perovskite. The formation of surface interaction leads to formation of hydrophobic π – π interactions on the surface. This lead to high stability of the new perovskite against humidity, temperature,

light irradiation. This work has been able to use simple chemicals to fortify the high efficiency $MAPbI_3$. The study has confirmed that not all the molecules can be suitable for substitution reaction to generate double organic perovskite. Even though this work was done under 60% relative humidity, the capped perovskite device achieved 11.38% efficiency for cost effective carbon-graphite counter electrode and solid-state CuSCN HTM with sandwich type architecture. The results point towards the fact that very high efficiency can be achieved if the devices are to be fabricated under standard conditions. The PA as capping agent for $MAPbI_3$ perovskite indicate great potential for the newly developed material not only in terms of efficiency solar cells, but also as ingredients for future optoelectronic. Therefore, we use this work to wake up awareness of the material scientists, to explore capping of perovskite as alternative means of prolong the material life and thus making them suitable for commercialization.

Acknowledgement

One of the authors, Ogunniran, K. O., expresses gratitude to CSIR, India and TWAS for financial support through TWAS-CSIR postdoctoral fellowship grant to carry out this work. The authors thank Dr. Vijayamohanan K Pillai, Director, CSIR-Central Electrochemical Research Institute, Karaikudi, India for his constant support and encouragement. The authors also thank all the technical staff of CSIR-Central Electrochemical Research Institute for their support to carry out characterization studies.

Appendix A. Supplementary material

Supplementary data associated with this article can be found in the online version at doi:10.1016/j.solmat.2018.11.041.

References

[1] M.A. Green, A. Ho-Baillie, H.J. Snaith, The emergence of perovskite solar cells, Nat. Photonics 8 (2014) 506–514.
[2] H.J. Snaith, Perovskites: the emergence of a new era for low-cost, high-efficiency solar cells, J. Phys. Chem. Lett. 4 (2013) 3623–3630.
[3] W.S. Yang, J.H. Noh, N.J. Jeon, Y.C. Kim, S. Ryu, J. Seo, S. Seok, High-performance photovoltaic perovskite layers fabricated through intramolecular exchange, Science 348 (2015) 1234–1237.
[4] P.K. Nayak, D.T. Moore, B. Wenger, S. Nayak, A.A. Haghighirad, A. Fineberg, N.K. Noel, O.G. Reid, G. Rumbles, P. Kukura, K.A. Vincent, H.J. Snaith, Mechanism for rapid growth of organic–inorganic halide perovskite crystals, Nat. Commun. 7 (2016) 13303.
[5] K. Hwang, Y.S. Jung, Y.J. Heo, F.H. Scholes, S.E. Watkins, J. Subbiah, D.J. Jones, D.Y. Kim, D. Vak, Toward large scale roll-to-roll production of fully printed perovskite solar cells, Adv. Mater. 27 (2015) 1241–1247.
[6] Y. Fu, H. Zhu, A.W. Schrader, D. Liang, Q. Ding, P. Joshi, L. Hwang, X.Y. Zhu, S. Jin, Nanowire lasers of formamidinium lead halide perovskites and their stabilized alloys with improved stability, Nano Lett. 16 (2016) 1000–1008.
[7] U. Bach, D. Lupo, P. Comte, J.E. Moser, F. Weissörtel, J. Salbeck, H. Spreitzer, M. Grätzel, Solid-state dye-sensitized mesoporous TiO_2 solar cells with high photon-to-electron conversion efficiencies, Nature 395 (1998) 583–585.
[8] T. Xu, L. Chen, Z. Guo, T. Ma, Strategic improvement of the long-term stability of perovskite materials and perovskite solar cells, Phys. Chem. Chem. Phys. 18 (2016) 27026–27050.
[9] S. Yang, W. Fu, Z. Zhang, H. Chen, C.–Z. Li, Recent advances in perovskite solar cells: efficiency, stability and lead-free perovskite, J. Mater. Chem. A 5 (2017) 11462–11482.
[10] S.F. Hoefler, G. Trimmel, T. Rath Monatsh, Progress on lead-free metal halide perovskites for photovoltaic applications: a review, Mon. Chem. - Chem. Mon. 148 (2017) 795–826.
[11] M.A. Green, K. Emery, Y. Hishikawa, W. Warta, E.D. Dunlop, D.H. Levi, A.W.H. Ho-Baillie, Solar cell efficiency tables (version 50), Progress. Photovolt. 25 (2017) 668–676.
[12] J.S. Manser, P.V. Kamat, Band filling with free charge carriers in organometal halide perovskites, Nat. Photonics 8 (2014) 737–743.
[13] N. Li, D. Baran, K. Forberich, F. Machui, T. Ameri, M. Turbiez, M. Carrasco-Orozco, M. Drees, A. Facchetti, F.C. Krebs, C.J. Brabeca, Towards 15% energy conversion efficiency: a systematic study of the solution-processed organic tandem solar cells based on commercially available materials, Energy Environ. Sci. 6 (2013) 3407–3413.
[14] J. You, L. Dou, K. Yoshimura, T. Kato, K. Ohya, T. Moriarty, K. Emery, C.-C. Chen, J. Gao, G. Li, Y. Yang, A polymer tandem solar cell with 10.6% power conversion efficiency, Nat. Commun. 4 (2013) 1446.
[15] X. Zhang, X. Ren, B. Liu, R. Munir, X. Zhu, D. Yang, J. Li, Y. Liu, D. Smilgies, R. Li, Z. Yang, T. Niu, X. Wang, A. Amassian, K. Zhao, S. Liu, Stable high efficiency two-dimensional perovskite solar cells via cesium doping, Energy Environ. Sci. 10 (2017) 2095–2102.
[16] J. Burschka, N. Pellet, S.J. Moon, R. Humphry-Baker, P. Gao, M.K. Nazeeruddin, M. Gratzel, Sequential deposition as a route to high-performance perovskite-sensitized solar cells, Nature 499 (2013) 316–319.
[17] B. Roose, A. Ummadisingu, J.C. Baena, M. Saliba, A. Hagfeldt, M. Graetzel, U. Steiner, A. Abate, Spontaneous crystal coalescence enables highly efficient perovskite solar cells, Nano Energy 39 (2017) 24–29.
[18] G.E. Eperon, T. Leijtens, K.A. Bush, R. Prasanna, T. Green, J.T. Wang, D.P. McMeekin, G. Volonakis, R.L. Milot, R. May, A. Palmstrom, D.J. Slotcavage, R.A. Belisle, J.B. Patel, E.S. Parrott, R.J. Sutton, W. Ma, F. Moghadam, B. Conings, A. Babayigit, H.G. Boyen, S. Bent, F. Giustino, L.M. Herz, M.B. Johnston, M.D. McGehee, H.J. Snaith, Perovskite-perovskite tandem photovoltaics with optimized band gaps, Science 354 (2016) 861–865.
[19] H. Tang, S. He, C. Peng, A short progress report on high-efficiency perovskite solar cells, Nanoscale Res. Lett. 12 (2017) 410.
[20] N.-G. Park, Perovskite solar cells: an emerging photovoltaic technology, Mater. Today 18 (2015) 65–72.
[21] H.X. Zhu, J.-M. Liu, Electronic structure of organometal halide perovskite $CH_3NH_3BiI_3$ and optical absorption extending to infrared region, Sci. Rep. 6 (2016) 37425.
[22] M. Petrović, V. Chellappan, S. Ramakrishna, Perovskites: solar cells & engineering applications – materials and device developments, Sol. Energy 122 (2015) 678–699.
[23] C. Yi, J. Luo, S. Meloni, A. Boziki, N. Ashari-Astani, C. Gratzel, S.M. Zakeeruddin, U. Rothlisberger, M. Gratzel, Entropic stabilization of mixed A-cation ABX_3 metal halide perovskites for high performance perovskite solar cells, Energy Environ. Sci. 9 (2016) 656–662.
[24] P.P. Boix, K. Nonomura, N. Mathews, S.G. Mhaisalkar, Current progress and future perspectives for organic/inorganic perovskite solar cells, Mater. Today 17 (2014) 16–23.
[25] D. Li, P. Liao, X. Shai, W. Huang, S. Liu, H. Li, Y. Shen, M. Wang, Recent progress on stability issues of organic–inorganic hybrid lead perovskite-based solar cells, RSC Adv. 6 (2016) 89356–89366.
[26] G. Niu, X. Guo, L. Wang, Review of recent progress in chemical stability of perovskite solar cells, J. Mater. Chem. A 3 (2015) 8970–8980.
[27] M.-H. Li, H.-H. Yeh, Y.-H. Chiang, U.-S. Jeng, C.-J. Su, H.-W. Shiu, Y.-J. Hsu, N. Kosugi, T. Ohigashi, Y.-A. Chen, P.-S. Shen, P. Chen, T.-F. Guo, Highly Effcient 2D/3D hybrid perovskite solar cells via low-pressure vapor-assisted solution process, Adv. Mater. 30 (2018) 1801401–1801413.
[28] N.K. Noel, A. Abate, S.D. Stranks, E.S. Parrott, V.M. Burlakov, A. Goriely, H.J. Snaith, Enhanced photoluminescence and solar cell performance via lewis base passivation of organic–inorganic lead halide perovskites, ACS Nano 8 (2014) 9815–9821.
[29] J.-W. Lee, Z. Dai, T.-H. Han, C. Choi, S.-Y. Chang, S.-J. Lee, N.D. Marco, H. Zhao, P. Sun, Y. Huang, Y. Yang, 2D perovskite stabilized phase-pure formamidinium perovskite solar cells, Nat. Commun. 9 (2018) 3021–3030.
[30] J.-F. Liao, H.-S. Rao, B.-X. Chen, D.-B. Kuang, C.-Y. Su, Dimension engineering on cesium lead iodide for efficient and stable perovskite solar cells, J. Mater. Chem. A 5 (2017) 2066–2072.
[31] J. Huang, Y. Yuan, Y. Shao, Y. Yan, Understanding the physical properties of hybrid perovskites for photovoltaic applications, Nat. Rev. Mater. 2 (2017) 17042.
[32] X. Zhao, H.-S. Kim, J.-Y. Seo, N.-G. Park, Effect of selective contacts on the thermal stability of perovskite solar cells, ACS Appl. Mater. Interfaces 9 (2017) 7148–7153.
[33] T. Leijtens, K. Bush, R. Cheacharoen, R. Beal, A. Bowring, M.D. McGehee, Towards enabling stable lead halide perovskite solar cells; interplay between structural, environmental, and thermal stability, J. Mater. Chem. A 5 (2017) 11483–11500.
[34] S. Sarang, S.B. Naghadeh, B. Luo, P. Kumar, E. Betady, V. Tung, M. Scheibner, J.Z. Zhang, S. Ghosh, Stabilization of the cubic crystalline phase in organometal halide perovskite quantum dots via surface energy manipulation, J. Phys. Chem. Lett. 8 (2017) 5378–5384.
[35] J. Zhou, J. Huang, Photodetectors based on organic–inorganic hybrid lead halide perovskites, Adv. Sci. 5 (2017) 1700256.
[36] G. Murugadoss, R. Thangamuthu, S.M.S. Kumar, Fabrication of $CH_3NH_3PbI_3$ perovskite-based solar cells: developing various new solvents for CuSCN hole transport material, Sol. Energy Mater. Sol. Cells 164 (2017) 56–62.
[37] N. Li, Z. Zhu, C. Chueh, H. Liu, B. Peng, A. Petrone, X. Li, L. Wang, A.K.-Y. Jen, Mixed cation $FA_xPEA_{1-x}PbI_3$ with enhanced phase and ambient stability toward high-performance perovskite solar cells, Adv. Energy Mater. 7 (2016) 1601307.
[38] L. Qiu, L.K. Ono, Y. Qi, Advances and challenges to the commercialization of organic–inorganic halide perovskite solar cell technology, Mater. Today Energy 7 (2017) 169–189.
[39] P.J. Linstrom, W.G. Mallard, National Institute of Standards and Technology, Gaithersburg MD, NIST Chemistry WebBook, NIST Standard Reference Database Number 69, ed., 20899, 2009.
[40] N. Ahn, K. Kwak, M.S. Jang, H. Yoon, B.Y. Lee, J.-K. Lee, P.V. Pikhitsa, J. Byun, M. Choi, Trapped charge-driven degradation of perovskite solar cells, Nat. Commun. 7 (2016) 13422.
[41] G. Kresse, J. Furthmüller, Efficient iterative schemes for ab initio total-energy calculations using a plane-wave basis set, Phys. Rev. B 54 (1996) 11169–11186.
[42] P.E. Blöchl, Projector augmented-wave method, Phys. Rev. B 50 (1994) 17953–17979.
[43] B.E. Cohen, M. Wierzbowska, L. Etgar, High efficiency quasi 2D lead bromide perovskite solar cells using various barrier molecules, Sustain. Energy Fuels 1

(2017) 1935–1943.
[44] H.–S. Kim, J.–Y. Seo, N.–G. Park, Impact of selective contacts on long-term stability of $CH_3NH_3PbI_3$ perovskite solar cells, J. Phys. Chem. C 120 (49) (2016) 27840–27848.
[45] G.P. Nagabhushana, R. Shivaramaiah, A. Navrotsky, Direct calorimetric verification of thermodynamic instability of lead halide hybrid perovskites, PNAS 113 (2016) 7717–7721.
[46] J. Qiu, Y. Qiu, K. Yan, M. Zhong, C. Mu, H. Yan, S. Yang, All-solid-state hybrid solar cells based on a new organometal halide perovskite sensitizer and one-dimensional TiO_2 nanowire arrays, Nanoscale 5 (2013) 3245–3248.
[47] E.J. Juarez-Perez, Z. Hawash, S.R. Raga, L.K. Ono, Y. Qi, Thermal degradation of $CH_3NH_3PbI_3$ perovskite into NH_3 and CH_3I gases observed by coupled thermogravimetry–mass spectrometry analysis, Energy Environ. Sci. 9 (2016) 3406–3410.
[48] J. Jagielski, S. Kumar, W.-Y. Yu, C. Shih, Layer-controlled two-dimensional perovskites: synthesis and optoelectronics, J. Mater. Chem. C 5 (2017) 5610–5627.
[49] Y. Zhang, J. Liu, Z. Wang, Y. Xue, Q. Ou, L. Polavarapu, J. Zheng, X. Qi, Q. Bao, Synthesis, properties, and optical applications of low-dimensional perovskites, Chem. Commun. 52 (2016) 13637–13655.
[50] H. Choi, J. Jeong, H. Kim, S. Kim, B. Walker, G. Kim, J.Y. Kim, Cesium-doped methylammonium lead iodide perovskite light absorber for hybrid solar cells, Nano Energy 7 (2014) 80–85.
[51] Y. Zhao, K. Zhu, Charge transport and recombination in perovskite $(CH_3NH_3)PbI_3$ sensitized TiO_2 solar cells, J. Phys. Chem. Lett. 4 (2013) 2880–2884.
[52] P. Fan, D. Gu, G.–X. Liang, J.–T. Luo, J.–L. Chen, Z.–H. Zheng, D.–P. Zhang, High-performance perovskite $CH_3NH_3PbI_3$ thin films for solar cells prepared by single-source physical vapour deposition, Sci. Rep. 6 (2016) 29910.
[53] C.N. Savory, A. Walsh, D.O. Scanlon, Can Pb-free halide double perovskites support high-efficiency solar cells? ACS Energy Lett. 1 (2016) 949–955.
[54] J. Endres, D.A. Egger, M. Kulbak, R.A. Kerner, L. Zhao, S.H. Silver, G. Hodes, B.P. Rand, D. Cahen, L. Kronik, A. Kahn, Valence and conduction band densities of states of metal halide perovskites: a combined experimental–theoretical study, J. Phys. Chem. Lett. 7 (2016) 2722–2729.
[55] M.A. Pérez-Osorio, R.L. Milot, M.R. Filip, J.B. Patel, L.M. Herz, M.B. Johnston, F. Giustino, Vibrational properties of the organic–inorganic halide perovskite $CH_3NH_3PbI_3$ from theory and experiment: factor group analysis, first-principles calculations, and low-temperature infrared spectra, J. Phys. Chem. C 119 (2015) 25703–25718.
[56] A.E. Williams, P.J. Holliman, M.J. Carnie, M.L. Davies, D.A. Worsley, T.M. Watson, Perovskite processing for photovoltaics: a spectro-thermal evaluation, J. Mater. Chem. A 2 (2014) 19338–19346.
[57] B. Philippe, B.–W. Park, R. Lindblad, J. Oscarsson, S. Ahmadi, E.M.J. Johansson, H. Rensmo, Chemical and electronic structure characterization of lead halide perovskites and stability behavior under different exposures – a photoelectron spectroscopy investigation, Chem. Mater. 27 (2015) 1720–1731.
[58] D.S. Bhachu, D.O. Scanlon, E.J. Saban, H. Bronstein, I.P. Parkin, C.J. Carmalt, R.G. Scalable route to $CH_3NH_3PbI_3$ perovskite thin films by aerosol assisted chemical vapour deposition, J. Mater. Chem. A 3 (2015) 9071–9073.
[59] F. Xu, T. Zhang, G. Li, Y. Zhao, Mixed cation hybrid lead halide perovskites with enhanced performance and stability, J. Mater. Chem. A 5 (2017) 11450–11461.
[60] J.P. Perdew, J.A. Chevary, S.H. Vosko, K.A. Jackson, M.R. Pederson, D.J. Singh, C. Fiolhais, Atoms, molecules, solids, and surfaces: applications of the generalized gradient approximation for exchange and correlation, Phys. Rev. B 46 (1992) 6671–6687.
[61] D. Prochowicz, M. Franckevicius, A.M. Cieslak, S.M. Zakeeruddin, M. Gr¨atzel, J. Lewinski, Mechanosynthesis of the hybrid perovskite $CH_3NH_3PbI_3$: characterization and the corresponding solar cell efficiency, J. Mater. Chem. A 3 (2015) 20772–20777.
[62] X. Tong, F. Lin, J. Wu, Z.M. Wang, High performance perovskite solar cells, Adv. Sci. 3 (2016) 1500201.
[63] F. Zhang, S. Wang, Y. Xiao, X. Li, Improvement in photovoltaic performance of perovskite solar cells by interface modification and co-sensitization with novel asymmetry 7-coumarinoxy-4-methyltetrasubstituted metallophthalocyanines, Syn. Met. 220 (2016) 187–193.
[64] Q. Chena, N.D. Marcoa, Y.M. Yang, T.–B. Song, C.–C. Chena, H. Zhaoa, Z. Hong, H. Zhoua, Y. Yang, Under the spotlight: the organic–inorganic hybrid halide perovskite for optoelectronic applications, Nano Today 10 (2015) 355–396.
[65] Z. Liu, B. Sun, T. Shi, Z. Tang, G. Liao, Enhanced photovoltaic performance and stability of carbon counter electrode based perovskite solar cells encapsulated by PDMS, J. Mater. Chem. A 4 (2016) 10700–10709.